

## Morphologies of monolayer graphene under indentation

This article has been downloaded from IOPscience. Please scroll down to see the full text article.

2011 Modelling Simul. Mater. Sci. Eng. 19 054004

(<http://iopscience.iop.org/0965-0393/19/5/054004>)

[View the table of contents for this issue](#), or go to the [journal homepage](#) for more

Download details:

IP Address: 130.203.253.40

The article was downloaded on 27/06/2011 at 03:49

Please note that [terms and conditions apply](#).

# Morphologies of monolayer graphene under indentation

Xu Huang and Sulin Zhang<sup>1</sup>

Department of Engineering Science and Mechanics, The Pennsylvania State University,  
University Park, PA 16802, USA

E-mail: [suz10@psu.edu](mailto:suz10@psu.edu)

Received 15 March 2011, in final form 26 May 2011

Published 23 June 2011

Online at [stacks.iop.org/MSMSE/19/054004](http://stacks.iop.org/MSMSE/19/054004)

## Abstract

We employ a quasi-continuum method to characterize the deformation morphologies of monolayer graphene under indentation. The method involves casting the atomistic interaction potentials into the constitutive relations at the continuum level, thereby facilitating large-scale simulations with atomistic fidelity. Our simulations mapped out different morphological phases under indentation, depending on the indentation depth, the graphene–substrate adhesion strength and the graphene size. We carefully characterized the rippling phase and found that the wave number of the periodic rippling is dependent on the graphene–substrate adhesion strength and the graphene size, but not on the indentation depth. The simulation results provide new insights into the structural instability of graphene.

(Some figures in this article are in colour only in the electronic version)

## 1. Introduction

Graphene, a monolayer of carbon atoms, exhibits many novel properties including the surprisingly high room-temperature electron mobility [1]. Owing to its large ratio of in-plane rigidity to bending rigidity [2], monolayer graphene is prone to deformation into the third dimension, featuring local sharp folds. Examples range from buckling of singled and multi-walled carbon nanotubes (CNTs) under compression [3, 4], torsion [5, 6] and bending [4, 7–12]; edge-stress induced graphene warping [13, 14], etc. Previous experimental studies have found that the mechanical deformation morphologies significantly influence the electronic properties of graphene [15–17], which has motivated extensive studies of morphological patterns of graphene under thermal and mechanical loadings [18–20].

<sup>1</sup> Author to whom any correspondence should be addressed.

Nanoindentation has been widely used to probe the materials properties of graphene sheets, including Young's modulus and tribological properties [2, 21]. In the settings of the experiment of Lee *et al* [2], monolayer graphene was carefully deposited on a substrate with periodically arranged holes of radius on the order of micrometers. Indentation at the center of the hole probes the elastic modulus and fracture strength of the graphene. Both atomistic and continuum models were used to interpret the experiment results. Yet both types of models suffer limitations. Continuum models [20, 22] with phenomenological constitutive relations fail to capture the intrinsic nonlinearity and finite-strain anisotropy of graphene, while the fully atomistic simulations [20] are computationally very demanding and thus inaccessible to the length scale in the experiment settings.

In this paper, we develop a quasi-continuum method to study the deformation morphologies of monolayer graphene under indentation. Compared with fully atomistic models, our simulation method dramatically reduces the computational cost and thus can access phenomena at a much larger scale, therefore facilitating the study of size-dependent deformation morphology of graphene. Our simulation method also has advantageous over continuum models since the constitutive relations in our quasi-continuum model are analytically casted from the interatomic interaction potentials. Using the quasi-continuum method, we show that monolayer graphene under indentation exhibits evolving morphologies, ranging from uniform deformation, wave-like rippling, to local shape buckling or fracture, depending on the substrate-graphene adhesion strength and the graphene size. Our detailed analysis of the rippling phase shows that the wave number of the rippling also scales with the substrate-graphene adhesion strength and the graphene size. These numerical observations are rationalized through energetics analysis.

The paper is organized as follows. In section 2, we will introduce the quasi-continuum method. In section 3, we will present the mechanical properties, the deformation morphologies and energetics of graphene under indentation. Discussions and conclusions are provided in section 4.

## 2. Methodology

We adopt the second-generation Brenner potential [23] to describe the C–C covalent interactions in the monolayer graphene, which takes the following form:

$$V_{\text{TB}} = \sum_i \sum_{j>i} [V^{\text{R}}(r_{ij}) - B_{ij}(\mathbf{r})V^{\text{A}}(r_{ij})], \quad (1)$$

where  $r_{ij}$  is the distance between atoms  $i$  and  $j$ ,  $V^{\text{R}}$  and  $V^{\text{A}}$  are the pairwise repulsive and attractive interactions, respectively,  $B_{ij}$  is the bond-order function that has a complicated dependence on the bond angles and bond lengths involving atoms  $i$  and  $j$ .

The nonbonding van der Waals (vdW) potential consists of two components: interactions between carbon atoms within the monolayer graphene and between the carbon atoms and the substrate. The former needs to be included when self-contact deformation modes such as rippling and buckling present. The vdW interaction between two carbon atoms is described by the Lennard-Jones (LJ) potential [24] as

$$V_{\text{GG}}(r) = \frac{\epsilon}{r_0^6} \left[ \frac{1}{2} \kappa^6 \left( \frac{r_0}{r} \right)^{12} - \left( \frac{r_0}{r} \right)^6 \right], \quad (2)$$

where  $r$  is the interatomic distance,  $\kappa = 2.7$  is a dimensionless constant,  $r_0 = 1.42 \text{ \AA}$  is the equilibrium bond length and  $\epsilon = 15.2 \text{ eV \AA}^6$ . The vdW interaction between the carbon atoms

in the graphene sheet and in the substrate can be also described by a generic LJ potential:

$$V_{GS}(r) = \epsilon' \left[ \left( \frac{r_0}{r} \right)^{12} - \left( \frac{r_0}{r} \right)^6 \right]. \quad (3)$$

Given the atom density of the substrate  $\rho$ , one can determine the interaction potential between a single carbon atom in the graphene and the substrate. Treating the substrate as an infinite surface with a hole, one has

$$\tilde{V}_{GS}(h; r_c; R) = \frac{\epsilon' \rho \pi r_0^2}{2} \left[ \frac{2}{5} \left( \frac{r_0}{h} \right)^{12} - \left( \frac{r_0}{h} \right)^6 \right] - \int_{\Omega_C} V_{GS}(r) d\Omega, \quad (4)$$

where  $h$  is the vertical distance between the atom and the substrate,  $r_c$  is the distance between the carbon atom and the center of the hole,  $R$  is the radius of the hole and  $\Omega_C$  is the surface region of the hole. The first term in the right-hand side of equation (4) is the interaction potential between a carbon atom and an infinite surface; the second term takes into account of the presence of the hole. One also follows that the graphene–substrate adhesion strength (energy per unit area) is  $\gamma = (\rho \pi r_0^2 / 2S_0) \epsilon'$ , where  $S_0 = (3\sqrt{3}/2) ||\mathbf{A}||^2$  is the area of the unit cell in the graphene lattice,  $\mathbf{A}$  is the lattice constant of the graphene in the undeformed configuration. We choose  $r_0 = 3.4 \text{ \AA}$  as the equilibrium distance between the carbon atom and infinitely large substrate, the same as the equilibrium gap between two graphene sheets.

We next analytically cast the atomistic interaction potentials into the continuum level constitutive relations. For the in-plane deformation energy of the monolayer graphene, the finite crystal elasticity theory of Arroyo and Belytschko [25, 26] links the kinematic descriptions on the atomic and continuum levels via the exponential Cauchy–Born hypothesis,

$$\mathbf{a} = \zeta(\mathbf{A}), \quad (5)$$

where  $\zeta$  is an exponential map that transforms the undeformed lattice vector  $\mathbf{A}$  into a deformed one  $\mathbf{a}$ . Through a local approximation of the exponential map, the deformed lattice vectors and the angles between two lattice vectors can be analytically represented in terms of the continuum deformation measures, i.e.  $\mathbf{C}$  and  $\mathbf{K}$ , the stretch and curvature tensors, respectively. Considering a representative unit cell of area  $S_0$  in the graphene lattice, the kinematic link allows analytically determining the hyperelastic strain energy from the underlying interatomic potentials as

$$W = W(\mathbf{C}; \mathbf{K}) = W[\mathbf{a}(\mathbf{C}; \mathbf{K}); \alpha(\mathbf{C}; \mathbf{K})], \quad (6)$$

where  $\mathbf{a}$  and  $\alpha$  represent generic lattice vectors and angles between lattice vectors, respectively. The continuum representation of the covalent binding energy for the graphene subject to the deformation map  $\phi$  that maps from the undeformed to deformed configurations is

$$E_G = \int_{\Omega_0} W\{\mathbf{C}[\phi(\mathbf{X})]; \mathbf{K}[\phi(\mathbf{X})]\} d\Omega_0, \quad (7)$$

where  $\mathbf{X}$  is a material point in the undeformed configuration and  $\Omega_0$  is the surface area of the graphene.

Homogenization of the discrete nonbonding energy between two unit cells of the graphene lattice gives rise to the vdW energy density:

$$\hat{V}_{GG}(r) = \left( \frac{2}{S_0} \right)^2 V_{GG}(r), \quad (8)$$

where  $r$  is the distance between two material points in the graphene. Note that the factor of two on the right-hand side of equation (8) comes from the fact that each unit cell contains

two nuclei. The continuum form of the nonbonding energy  $E_{GG}$  is a double integral over the graphene surface:

$$E_{GG} = \frac{1}{2} \int_{\Omega_{0X}} \int_{\Omega_{0Y}} \hat{V}_{GG}[||\phi(\mathbf{X}) - \phi(\mathbf{X}')||] d\Omega_{0X} d\Omega_{0Y}, \quad (9)$$

where  $\mathbf{X}$  and  $\mathbf{Y}$  are the two material points in the monolayer graphene. Note that in computing the self-contacting vdW interaction energy, two cutoff radii are used. The lower cutoff radius excludes the covalent interaction region ( $\sim 2.0 \text{ \AA}$ ), while the upper cutoff radius is typically taken to be 1.0 nm.

Homogenization of the discrete graphene–substrate vdW energy gives rise to the vdW energy density as

$$\hat{V}_{GS}(h; r_C; R) = \left( \frac{2}{S_0} \right) \tilde{V}_{GS}(h; r_C; R). \quad (10)$$

The nonbonded energy between the graphene and substrate is then

$$E_{GS} = \int_{\Omega_0} \hat{V}_{GS} [h(\phi(\mathbf{X})); r_C(\phi(\mathbf{X})); R] d\Omega_0. \quad (11)$$

Note that  $h$  and  $r_C$  are both determined by the position of the material point  $\phi(\mathbf{X})$  in the deformed configuration.

The total energy of the system is

$$E_{\text{total}} = E_G + E_{GG} + E_{GS}. \quad (12)$$

Based on the coarse-grained constitutive relations for both the bonding and nonbonding interactions, the graphene is discretized by finite elements. The model with the first two energy terms has been extensively tested [3–5, 7, 9, 11, 25, 26] and demonstrated its atomic accuracy. In addition, the computational efficiency is improved by about two orders of magnitude as compared with its atomistic counterpart. It should be pointed out that the quasi-continuum method described here is incapable of studying the deformation of defected CNTs, which has been a topic of active research for the last decade [27–35].

### 3. Results and discussion

This section presents the simulation results on the deformation morphologies and energetics of monolayer graphene under indentation. Our numerical setting involves a square graphene sheet adhered on the substrate with a circular hole. The circular hole and the graphene are centered. The diameters of the circular holes are chosen to be 100, 200, 300, 400 and 500 nm, 80% of the corresponding side lengths of the graphene sheets. To begin with, the graphene is fully relaxed free of any constraints using the limited-memory Broyden–Fletcher–Goldfarb–Shanno (BFGS) algorithm [36]. A rigid indenter is then moved downward incrementally to indent the graphene, followed by a geometry optimization to the local energy minimum configuration at each step. The radius of the indenter  $R_I$  is chosen to be 1% of that of the substrate hole. The interaction between the indenter and the graphene is modeled by an external repulsive potential as

$$V_{\text{ext}}(r) = AH(R_I - r)(R_I - r)^3, \quad (13)$$

where  $A$  is a force constant and  $H(R_I - r)$  is the step function. We set  $A = 6.25 \times 10^3 \text{ eV \AA}^{-3}$ . The deformation morphology, the energy distribution and the applied indentation force are computed at each loading step.

Figures 1(a)–(c) show the deformation morphologies of the square graphene of side length of 125 nm under indentation. The graphene–substrate adhesion strength is  $1.6 \text{ eV nm}^{-2}$ .

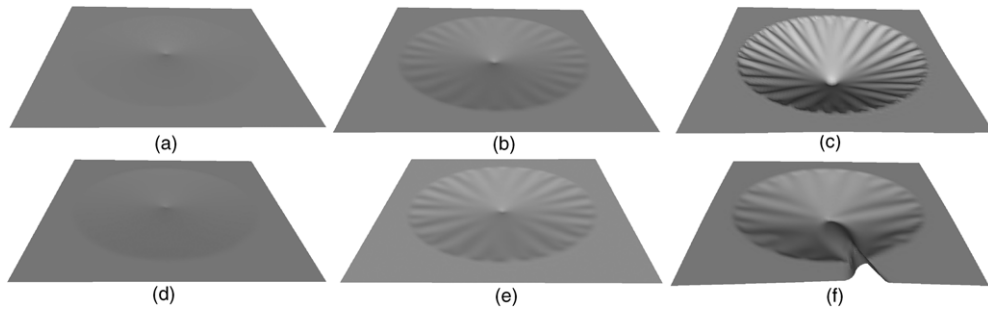


**Figure 1.** Deformation morphologies of an indented graphene of side length of 125 nm (hole diameter: 100 nm). (a)–(c) Deformation morphologies of graphene with graphene–substrate adhesion strength of  $1.6 \text{ eV nm}^{-2}$ . From (a) to (c), the indentation depths are 2 nm, 5 nm and 19 nm, respectively. (d)–(f) Deformation morphologies of graphene with graphene–substrate adhesion strength of  $0.4 \text{ eV nm}^{-2}$ . From (d) to (f), the indentation depths are 2 nm, 5 nm and 15 nm, respectively.

At small indentation depth ( $d = 2 \text{ nm}$ ), the graphene deforms uniformly, as shown in figure 1(a). With increasing indentation depth, periodic rippling develops (figures 1(b) and (c)). The rippling modifies the otherwise compressive mode into the out-of-plane bending mode, since the latter is energetically more favorable. The rippling diminishes close to the center of the graphene, indicating that the graphene in the center region undergoes biaxial stretch. At the same time, small secondary rippling appears at the edge of the circular hole. Upon rippling, the graphene–substrate separation near the edges of the hole increases, giving rise to larger substrate–graphene vdW energy. Therefore, rippling is penalized by the graphene–substrate decohesion energy. Fracture of the graphene occurs at the indentation depth of 19 nm, suggested by failing in obtaining a local energy minimum. The deformation morphologies of graphene with adhesion strength of  $0.4 \text{ eV nm}^{-2}$  are shown in figures 1(d)–(f). Different from the morphology evolution of graphene with high adhesion strength, beyond periodic rippling phase, graphene with low adhesion strength buckles locally without fracture.

Under indentation, the graphene tends to flow radially toward the center of the hole, creating excessive surface area of the highly stretched region and thereby releasing the in-plane stretching energy. The deformation morphology of the graphene depends on the amount of the flow-in displacement  $\delta$  of the graphene into the center of the hole. Figure 2 plots the flow-in displacement of the graphene of 125 nm in size length. Due to the geometrical asymmetry in the radial direction, the flow-in displacement is nonuniform, and is larger at the central region of the side than at the corner region, as shown in figure 2(a). Figure 2(b) plots the flow-in displacement at the central region of the graphene side as a function of indentation depth at different graphene–substrate adhesion strength. For all the adhesion strengths, the flow-in displacement homogeneously increases at the initial stage of indentation. During this stage, the deformation morphology evolves from uniform deformation phase to rippling phase. The smooth transition indicates the energetic closeness of these two deformation phases. At a critical indentation depth, the flow-in displacement jumps sharply, indicating the occurrence of buckling. With increasing graphene–substrate adhesion strength, the critical indentation depth increases monotonically, as observed from figure 2(b).

Figure 3(a) shows the rippling amplitude of graphene at the radial coordinate  $r = 33.33 \text{ nm}$ . The side length of the graphene is 125 nm, and the graphene–substrate adhesion strength is  $0.4 \text{ eV nm}^{-2}$ . At the indentation depth of  $d = 3 \text{ nm}$ , the rippling amplitude is nearly zero (blue line in figure 3(a)), indicating the absence of rippling. The rippling amplitude is  $\sim 0.1 \text{ nm}$  at the indentation depth of 6 nm. With further increasing indentation depth, the

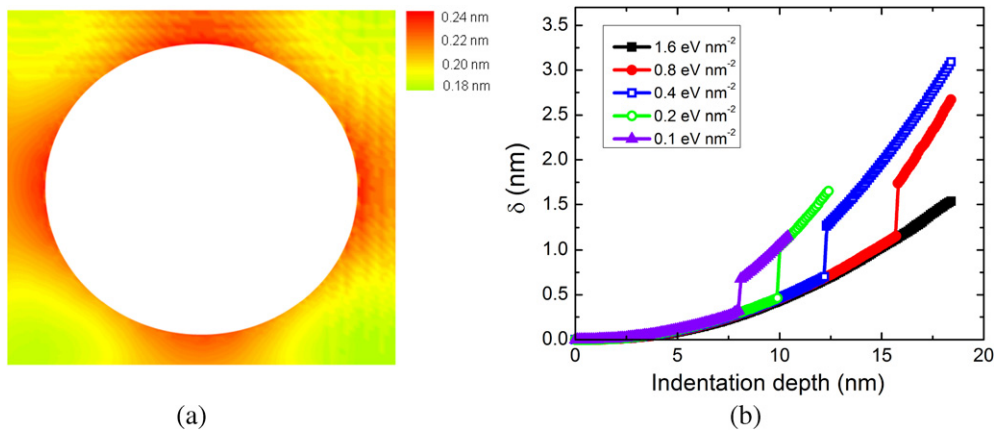


**Figure 2.** The flow-in displacement of the graphene of 125 nm in size length. (a) The nonuniformity of the flow-in displacement; (b) The flow-in displacement at different indentation depths.

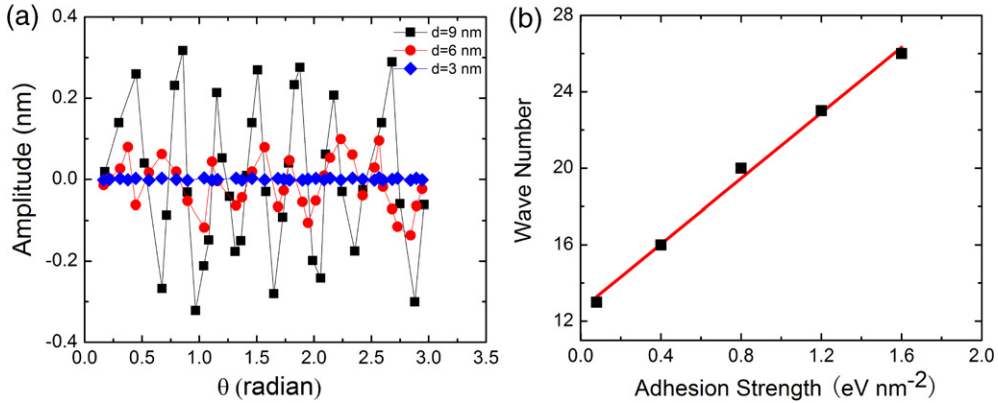


**Figure 3.** (a) Rippling amplitudes at  $r = 33.33$  nm of graphene adhered to the substrate with the hole of 100 nm diameter. (b) Wave number of the rippled graphene at different adhesion strengths.

rippling amplitude increases. For example, the rippling amplitude is  $\sim 0.3$  nm at the indentation depth of 9 nm. However, the wave number of graphene under indentation is nearly independent of the indentation depth. Here, the wave number is determined based on the primary rippling, not on the secondary rippling near the edge of the hole. Figure 3(a) clearly shows that the rippling is indeed nearly periodic. Figure 3(b) shows that the wave number of the periodic rippling nearly linearly scales with the graphene–substrate adhesion strength. The red straight line in the figure is the linear fitting of the data points. The increase of the wave number with the adhesion strength can be understood from the relative significance of the graphene–substrate adhesion energy and the deformation energy of the graphene. At larger adhesion strength, the amount of flow-in graphene area is smaller due to the higher graphene–substrate decohesion energy. The deformation morphology under this condition prefers smaller rippling amplitudes, giving rise to a larger wave number.

Figures 4(a)–(d) display the energy density distribution of the graphene at different indentation depths. In the initial configuration of the graphene (figure 4(a)), the surrounding region adhering to the substrate has a lower energy density than the suspended region. As the indenter moves down, the high energy density region (red region) expands radially from the

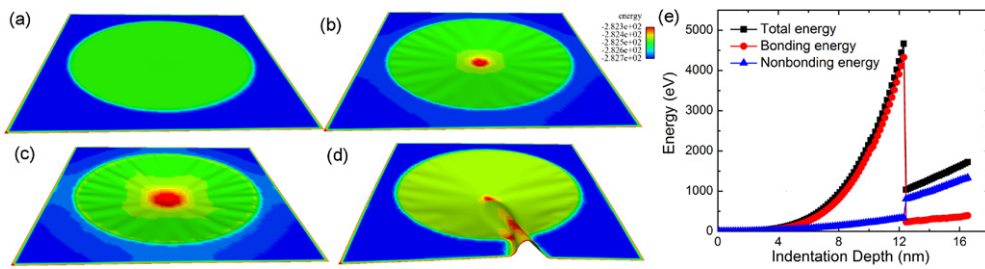


**Figure 4.** (a)–(d) Energy density distribution of graphene of side length of 125 nm (red for higher energy state and blue for lower). The adhesion strength is  $0.4 \text{ eV nm}^{-2}$ . From (a) to (d), the indentation depths are 0, 5, 10 and 15 nm, respectively. (e) Energetics of graphene under indentation (energy bar unit  $\text{eV nm}^{-2}$ ).

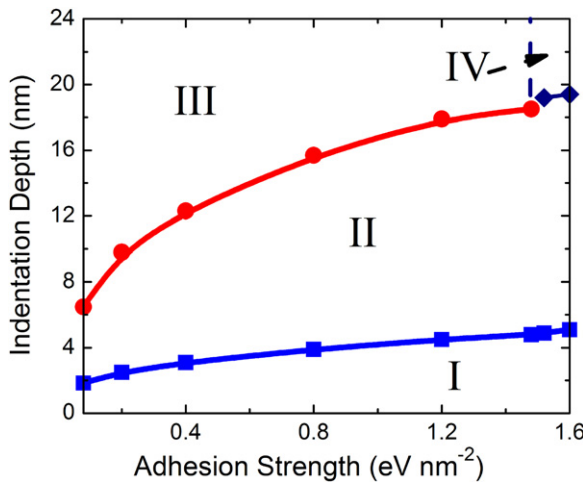
center, as shown in figures 4(b) and (c). The high energy density region around the indenter is caused by the large local elastic stretch. We also observed that the graphene deforms appreciably at the center of the four edges that adhere to the substrate as the indentation depth increases (light blue region in figure 4(c)). However, the corner regions of the graphene remain nearly perfectly adhered to the substrate. Figure 4(d) shows the energy density distribution of the buckled configuration. The local buckling releases the energy not only in the central region around the indenter but also at the edges of the graphene. As a result, the energy distribution over the suspended region of the graphene is more uniform. Figure 4(e) plots the energy variations at different indentation depths, where the bonding energy is comprised of in-plane stretching energy and out-of-plane bending energy. From an energetics point of view, the transition from the uniform deformation phase to rippling phase is indeed smooth, consistent with conclusion from the flow-in displacement. It is clearly seen that after buckling, the bonding energy decreases while the nonbonding vdW energy increases, both sharply. The total system energy decreases after buckling due to the relaxation of the stretched deformation.

Figure 5 plots the morphological phase diagram of the graphene under indentation, where the regimes of the uniformly deformed (I), rippling (II), buckling (III) and fracture (IV) phases are indicated in the space of the indentation depth and graphene–substrate adhesion strength. It is found that when the adhesion strength is smaller than  $1.5 \text{ eV nm}^{-2}$ , the deformation morphology evolves from the uniform pattern to the rippling and finally to the buckling pattern with increasing indentation depth. The critical indentation depth at the onset of instability for these three patterns increases with increasing adhesion strength. When the adhesion strength approaches  $1.5 \text{ eV nm}^{-2}$ , the fracture phase replaces the buckling phase in the diagram. It should be noted that the maximum adhesion strength used in this study is  $1.6 \text{ eV nm}^{-2}$ , which is the adhesion strength between two graphene sheets. For the adhesion strength larger than  $1.6 \text{ eV nm}^{-2}$ , it is expected that the morphological evolution will follow the path from the uniformly deformed pattern to the fracture pattern.

Figures 6(a)–(d) show the deformation morphologies of graphene of different sizes under indentation. The side lengths of the graphene from (a) to (d) are 125 nm, 250 nm, 375 nm, and 500 nm, respectively. The graphene–substrate adhesion strength is  $0.8 \text{ eV nm}^{-2}$ . The rippling patterns in these different sized graphene sheets are similar, and the rippling wave number increases nearly linearly with the graphene size, as shown in figure 6(e).

#### 4. Conclusions

In conclusion, our large-scale quasi-continuum simulations observed multiple morphological deformation phases in indented monolayer graphene, depending on the indentation depth



**Figure 5.** Morphological phase diagram of graphene under indentation. I: uniformly deformed phase; II: rippling phase; III: buckling phase; IV: fracture phase.

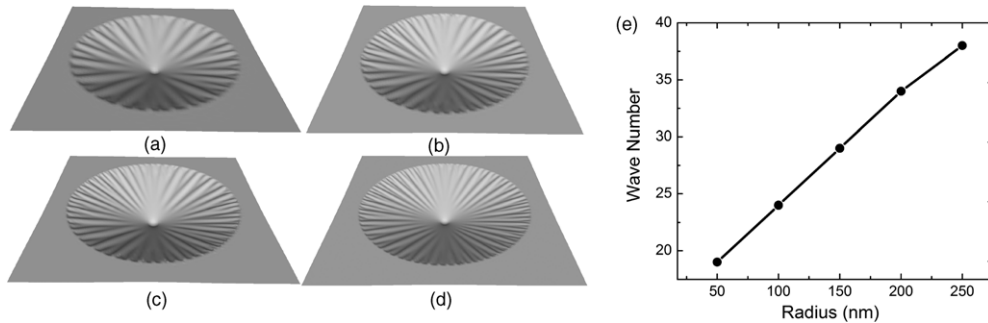


**Figure 6.** (a)-(d) Deformation morphologies of graphene under indentation. From (a) to (d), the side lengths of the graphene are 125 nm, 250 nm, 375 nm and 500 nm, respectively; the diameter of the hole is 80% of the side length. (e) The wave number of graphene scales with the side length.

and the substrate–graphene adhesion strength. Our energetics analysis suggests that the morphological phase transition at different loading regimes is a result of interplay of the in-plane deformation energy and graphene–substrate decohesion energy. The rippling wave number of the indented graphene linearly scales with the adhesion strength and the graphene size. This simple scaling law calls for theoretical analysis of the energetics of indented graphene. The multiple morphological phases alter the electronic-magnetic properties. The indented graphene thus can be used as a general experimental setting for the study of mechanical-electronic coupling.

## References

- [1] Geim A K and Novoselov K S 2007 The rise of graphene *Nature Mater.* **6** 183–91
- [2] Lee C, Wei X D, Kysar J W and Hone J 2008 Measurement of the elastic properties and intrinsic strength of monolayer graphene *Science* **321** 385–8
- [3] Huang X, Yuan H Y, Hsia K J and Zhang S L 2010 Coordinated buckling of thick multi-walled carbon nanotubes under uniaxial compression *Nano Res.* **3** 32–42

- [4] Huang X, Yuan H Y, Liang W T and Zhang S L 2010 Mechanical properties and deformation morphologies of covalently bridged multi-walled carbon nanotubes: multiscale modeling *J. Mech. Phys. Solids* **58** 1847–62
- [5] Huang X, Zou J and Zhang S L 2008 Bilinear responses and rippling morphologies of multiwalled carbon nanotubes under torsion *Appl. Phys. Lett.* **93** 031915
- [6] Zou J, Huang X, Arroyo M and Zhang S L 2009 Effective coarse-grained simulations of super-thick multi-walled carbon nanotubes under torsion *J. Appl. Phys.* **105** 033516
- [7] Arias I and Arroyo M 2008 Size-dependent nonlinear elastic scaling of multiwalled carbon nanotubes *Phys. Rev. Lett.* **100** 085503
- [8] Arroyo M and Arias I 2008 Rippling and a phase-transforming mesoscopic model for multiwalled carbon nanotubes *J. Mech. Phys. Solids* **56** 1224–44
- [9] Arroyo M and Belytschko T 2003 Nonlinear mechanical response and rippling of thick multiwalled carbon nanotubes *Phys. Rev. Lett.* **91** 215505
- [10] Cao G X and Chen X 2006 Buckling of single-walled carbon nanotubes upon bending: molecular dynamics simulations and finite element method *Phys. Rev. B* **73** 155435
- [11] Huang X and Zhang S L 2010 Load-driven morphological evolution in covalently bridged multiwalled carbon nanotubes *Appl. Phys. Lett.* **96** 203106
- [12] Li X Y, Yang W and Liu B 2007 Bending induced rippling and twisting of multiwalled carbon nanotubes *Phys. Rev. Lett.* **98** 205502
- [13] Shenoy V B, Reddy C D, Ramasubramaniam A and Zhang Y W 2008 Edge-stress-induced warping of graphene sheets and nanoribbons *Phys. Rev. Lett.* **101** 245501
- [14] Shenoy V B, Reddy C D and Zhang Y W 2010 Spontaneous curling of graphene sheets with reconstructed edges *Acs Nano* **4** 4840–4
- [15] Tombler T, Zhou C and Alexseyev L 2000 Reversible electromechanical characteristics of carbon nanotubes under local-probe manipulation *Nature* **405** 769–72
- [16] Crespi V H, Cohen M L and Rubio A 1997 In situ band gap engineering of carbon nanotubes *Phys. Rev. Lett.* **79** 2093–6
- [17] Hall A R, Falvo M R, Superfine R and Washburn S 2007 Electromechanical response of single-walled carbon nanotubes to torsional strain in a self-contained device *Nature Nanotechnol.* **2** 413–6
- [18] Bao W Z, Miao F, Chen Z, Zhang H, Jang W Y, Dames C and Lau C N 2009 Controlled ripple texturing of suspended graphene and ultrathin graphite membranes *Nature Nanotechnol.* **4** 562–6
- [19] Levy N, Burke S A, Meaker K L, Panlasigui M, Zettl A, Guinea F, Neto A H C and Crommie M F 2010 Strain-induced pseudo-magnetic fields greater than 300 Tesla in graphene nanobubbles *Science* **329** 544–7
- [20] Wang C Y, Mylvaganam K and Zhang L C 2009 Wrinkling of monolayer graphene: a study by molecular dynamics and continuum plate theory *Phys. Rev. B* **80** 155445
- [21] Lee C, Li Q Y, Kalb W, Liu X Z, Berger H, Carpick R W and Hone J 2010 Frictional characteristics of atomically thin sheets *Science* **328** 76–80
- [22] Lee C, Wei X D, Li Q Y, Carpick R, Kysar J W and Hone J 2009 Elastic and frictional properties of graphene *Phys. Status Solidi B—Basic Solid State Phys.* **246** 2562–7
- [23] Brenner D W, Shenderova O A, Harrison J A, Stuart S J, Ni B and Sinnott S B 2002 A second-generation reactive empirical bond order (REBO) potential energy expression for hydrocarbons *J. Phys.: Condens. Matter* **14** 783–802
- [24] Girifalco L A, Hodak M and Lee R S 2000 Carbon nanotubes, buckyballs, ropes, and a universal graphitic potential *Phys. Rev. B* **62** 13104–10
- [25] Arroyo M and Belytschko T 2002 An atomistic-based finite deformation membrane for single layer crystalline films *J. Mech. Phys. Solids* **50** 1941–77
- [26] Arroyo M and Belytschko T 2004 Finite crystal elasticity of carbon nanotubes based on the exponential Cauchy–Born rule *Phys. Rev. B* **69** 115415
- [27] Belytschko T, Xiao S P, Schatz G C and Ruoff RS 2002 Atomistic simulations of nanotube fracture *Phys. Rev. B* **65** 235430
- [28] Dumitrica T, Hua M and Yakobson B I 2006 Symmetry-, time-, and temperature-dependent strength of carbon nanotubes *Proc. Natl Acad. Sci. USA* **103** 6105–9
- [29] Khare R, Mielke S L, Paci J T, Zhang S L, Ballarini R, Schatz G C and Belytschko T 2007 Coupled quantum mechanical/molecular mechanical modeling of the fracture of defective carbon nanotubes and graphene sheets *Phys. Rev. B* **75** 075412
- [30] Mielke S L, Troya D, Zhang S, Li J L, Xiao S P, Car R, Ruoff R S, Schatz G C and Belytschko T 2004 The role of vacancy defects and holes in the fracture of carbon nanotubes *Chem. Phys. Lett.* **390** 413–20
- [31] Mielke S L, Zhang S, Khare R, Ruoff R S, Belytschko T and Schatz G C 2007 The effects of extensive pitting on the mechanical properties of carbon nanotubes *Chem. Phys. Lett.* **446** 128–32

- [32] Zhang S and Zhu T 2007 Atomic geometry and energetics of carbon nanotube necking *Phil. Mag. Lett.* **87** 567–74
- [33] Zhang S L, Mielke S L, Khare R, Troya D, Ruoff R S, Schatz G C and Belytschko T 2005 Mechanics of defects in carbon nanotubes: atomistic and multiscale simulations *Phys. Rev. B* **71** 115403
- [34] Zhang S L, Zhu T and Belytschko T 2007 Atomistic and multiscale analyses of brittle fracture in crystal lattices *Phys. Rev. B* **76** 094114
- [35] Terdalkar S S, Huang S, Yuan H Y, Rencis J J, Zhu T and Zhang S L 2010 Nanoscale fracture in graphene *Chem. Phys. Lett.* **494** 218–22
- [36] Liu D C and Nocedal J 1989 On the limited memory bfgs method for large-scale optimization *Math. Programming* **45** 503–28